Organotin-oxomolybdate coordination polymers

$$2\,R_3SnCl + Na_2[MoO_4] \xrightarrow[Me_2CO]{H_2O} [(R_3Sn)_2MoO_4]\cdot nH_2O\downarrow + 2\,NaCl$$

R = methyl, *n*-butyl, cyclohexyl, phenyl, benzyl

EXAFS, FTIR, FT Raman,

MAS NMR (^{13}C, ^{119}Sn)

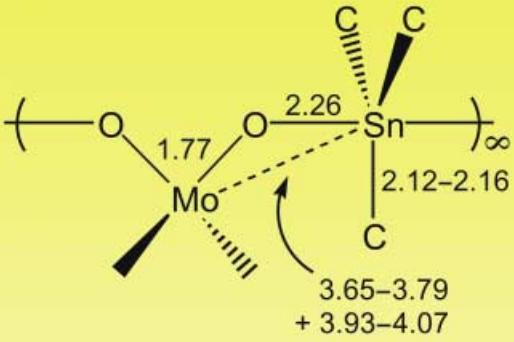

A model reaction relevant to the production of low-sulfur diesel by oxidative desulfurization

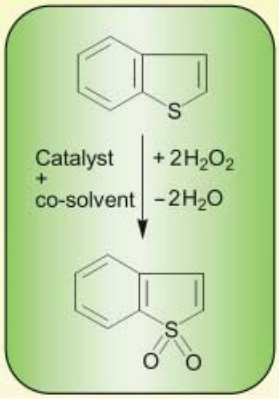

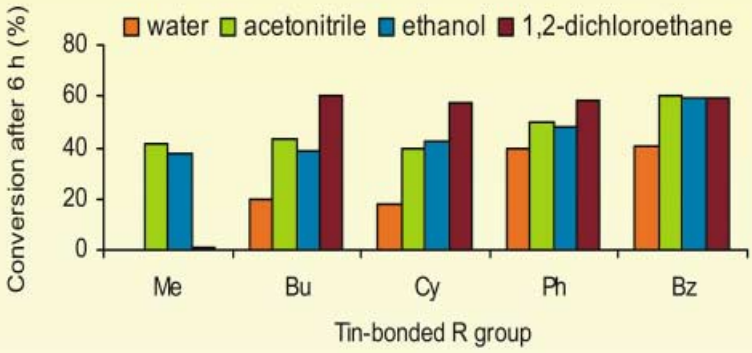

For more information please see the following pages.

 DOI: 10.1002/chem.200204399

Preparation and Characterization of Organotin – Oxomolybdate Coordination Polymers and Their Use in Sulfoxidation Catalysis

Marta Abrantes,[a] Anabela A. Valente,[b] Martyn Pillinger,[b] Isabel S. Gonçalves,*[b] João Rocha,[b] and Carlos C. Romão*[a]

Abstract: The organotin – oxomolybdates $[(R_3Sn)_2MoO_4]\cdot n\,H_2O$ (R = methyl, *n*-butyl, cyclohexyl, phenyl, benzyl) have been prepared and tested as catalysts for the oxidation of benzothiophene with aqueous hydrogen peroxide, at 35 °C and atmospheric pressure. In all cases, the 1,1-dioxide was the only observed product. The kinetic profiles depend on the nature of the tin-bound R group and also on the addition of a co-solvent. For the tribenzyltin derivative, the apparent activation energies for sulfoxidation as a function of the co-solvent are in the order 1,2-dichloroethane (5 kcal mol^{-1}) < ethanol < acetonitrile < water (27 kcal mol^{-1}). The solid could be recovered by centrifugation from the three-phase (solid – liquid – liquid) system containing 1,2-dichloroethane. The catalyst was reused in a second reaction cycle with no significant loss of activity. Increasing the oxidant/substrate ratio from 2:1 to 6:1 allows the corresponding sulfone to be obtained in quantitative yield within 24 h. Changing the nature of the tin-bound R group in the catalyst precursors modifies their physical properties and hence their catalytic performance. The variation in hydrophobic/hydrophilic character is important, since the Me, *n*Bu and Cy derivatives crystallize as anhydrous compounds, whereas the other two derivatives are hydrates. The polymers also have different structures, as evidenced by X-ray powder diffraction. Mo *K*-edge and Sn *K*-edge EXAFS spectroscopy confirmed that the structures arise from the self-assembly of tetrahedral $[MoO_4]^{2-}$ subunits and $[R_3Sn]^+$ spacers. The Mo ··· Sn separation in the trimethyltin derivative is a uniform 3.84 Å. By contrast, the EXAFS results revealed the coexistence of short (3.67 – 3.79 Å) and long (3.93 – 4.07 Å) Mo ··· Sn separations in the other coordination polymers. The catalyst precursors were also characterized in the solid state by thermogravimetric analysis, FTIR, and Raman spectroscopy, and MAS NMR (^{13}C, ^{119}Sn) spectroscopy.

Keywords: EXAFS spectroscopy · molybdenum · polymerization · sulfoxidation · tin

Introduction

In North America and Europe, the acceptable levels of sulfur in liquid hydrocarbon fuels are continually on the decrease, driven in part by the need to limit emissions of the oxides of sulfur which lead to acid rain, atmospheric ozone, and smog.[1] New, highly efficient and cost-effective desulfurization technologies are therefore required. Existing catalytic hydrodesulfurization processes are problematic because of the high temperatures and pressures required, the high hydrogen consumption, and the difficulty in removing certain refractory sulfides such as benzothiophene, dibenzothiophene, and 4,6-dimethyldibenzothiophene.[1, 2] To eliminate undesirable sulfur compounds or to convert them into more innocuous forms, various nonconventional processes have been employed or are being investigated, such as physical extraction with a liquid, selective adsorption on zeolites, and liquid-phase oxidative desulfurization.[3] In the last case, various types of oxidants are used, including hydrogen peroxide, ozone, *t*BuOOH, oxygen, and peracids. The liquid oxidation process with H_2O_2 produces sulfoxides (1-oxides) and sulfones (1,1-dioxides) that can be separated physically and processed downstream (sulfones can, for example, be used as surfactants). Near-atmospheric pressures and mild temperatures are used, and there is no need for hydrogen. Furthermore, H_2O_2 is economically attractive and eco-compatible as the oxidant, since water is the only chemical by-product formed from its decomposition during oxidative transformations. The oxidation of thiophene derivatives with H_2O_2 is known to take place over a limited range of metal-containing catalyst systems, such

[a] Prof. Dr. C. C. Romão, Dipl.-Chem. M. Abrantes
Instituto de Tecnologia Química e Biológica
da Universidade Nova de Lisboa
Quinta do Marquês, 2781-901 Oeiras (Portugal)
Fax: (+351) 21-4411277
E-mail: ccr@itqb.unl.pt

[b] Prof. Dr. I. S. Gonçalves, Dr. A. A. Valente, Dr. M. Pillinger, Prof. Dr. J. Rocha
Department of Chemistry, CICECO
University of Aveiro, 3810-193 Aveiro (Portugal)
E-mail: igoncalves@dq.ua.pt

Supporting information for this article is available on the WWW under http://www.wiley-vch.de/home/chemistry/ or from the author.

DOI: 10.1002/chem.200204399

as methyltrioxorhenium(VII),[4] polyoxometalates,[5] and titanium-containing molecular sieves.[6]

Recently, we found that organotin – oxometalate coordination polymers $[(n\mathrm{Bu_3Sn})_2\mathrm{MO_4}]$ (M = Mo, W) exhibit good catalytic activity for H_2O_2-based oxidations (epoxidation of olefins) at room temperature and atmospheric pressure.[7] With appropriate adjustment of the reaction conditions these materials become insoluble and act as heterogeneous catalysts, which are easily separated from the reaction products by centrifuging and can be reused without significant loss of activity. The tri-*n*-butyltin derivatives belong to a wider family of materials,[8] general formula $[(\mathrm{R_3E})_2\mathrm{MO_4}]$ (R = Me, Et, *n*Pr, *n*Bu, Ph; E = Sn, Pb; M = Mo, W). These compounds are accessible by precipitation from aqueous solution, using the starting materials $\mathrm{R_3ECl}$ and $\mathrm{NaMO_4 \cdot 2H_2O}$. Apart from the trimethyltin – oxomolybdate analogue, which was characterized by single-crystal X-ray diffraction, the organotin – oxometalate materials have not yet been characterized in detail. $[(\mathrm{Me_3Sn})_2\mathrm{MoO_4}]$ has a layered structure built up of tetrahedral MoO_4 and trigonal-bipyramidal $\mathrm{Me_3SnO_2}$ units (with shared oxygen atoms).[8] It is surprising that the catalytic properties of these polymers have not been investigated seriously. Encouraged by our recent findings with the tri-*n*-butyltin derivative, we now report on the oxidation of benzothiophene, chosen as a model substrate, by aqueous H_2O_2 in the presence of the organotin – oxomolybdates $[(\mathrm{R_3Sn})_2\mathrm{MoO_4}]$ [R = Me, *n*Bu, cyclohexyl (Cy), Ph, benzyl (Bz)]. The precursors have been characterized extensively, and we have studied the influence of the nature of the solvent, the tin-bound R group, the reaction temperature, and the oxidant concentration on the catalytic reaction.

Results and Discussion

Synthesis and characterization of catalyst precursors:

The organotin – oxomolybdates $[(\mathrm{R_3Sn})_2\mathrm{MoO_4}] \cdot n\,\mathrm{H_2O}$ were obtained as analytically pure precipitates by addition of a saturated aqueous solution of $\mathrm{Na_2MoO_4 \cdot 2H_2O}$ to a solution/suspension of $\mathrm{R_3SnCl}$ in either water (**1**, **2**) or acetone (**3** – **5**) at room temperature [Eq. (1), in which R = Me (**1**), *n*Bu (**2**), Cy (**3**), Ph (**4**), Bz (**5**)].

$$2\mathrm{R_3SnCl} + \mathrm{Na_2[MoO_4]} \xrightarrow[\mathrm{Me_2CO}]{\mathrm{H_2O}} [(\mathrm{R_3Sn})_2\mathrm{MoO_4}] \cdot n\mathrm{H_2O}\downarrow + 2\mathrm{NaCl} \quad (1)$$

R = Me (**1**), *n*Bu (**2**), Cy (**3**), Ph (**4**), Bz (**5**)

Elemental analysis repeatedly indicated that **1** – **3** are anhydrous compounds ($n = 0$), whereas **4** and **5** contain approximately two and four water molecules per formula unit, respectively. Thermogravimetric analysis (TGA) measurements under N_2 provided supporting evidence for the presence of nonremovable H_2O molecules in **4** and **5** (at least after prolonged drying in vacuo at room temperature). Thus, upon heating, the weight of compounds **1** – **3** remains constant from 25 °C to at least 100 °C (150 °C for **3**). Compound **4**, however, loses 1.7 % of its initial weight in the temperature range 25 – 100 °C. The tribenzyltin derivative **5** starts to melt at 85 °C and then produces a foam at 108 °C. A steady mass loss of 6.5 % occurs between 25 and 125 °C; this is consistent with the presence of four H_2O molecules per formula unit. Upon further heating, decomposition starts at about 150 °C and 38 % weight loss takes place up to 275 °C. The thermal behavior of **5** is quite different from that of **1** – **4**, which tend to melt and decompose above 200 °C (Table 1).

The identity and purity of the trimethyltin derivative **1** were confirmed by comparison of experimental and calculated X-ray powder diffraction (XRPD) patterns (see Supporting Information). Compounds **2**, **3**, and **5** give rise to XRPD patterns consisting of relatively sharp reflections, indicating a polycrystalline nature (see Supporting Information). The patterns are quite different from that of **1**, suggesting that the tin-bound R group exerts a considerable structure-directing influence, as observed previously for coordination polymers $[(\mathrm{R_3Sn})_3\mathrm{Rh(SCN)_6}]$ (R = Me, Et, *n*Pr, *n*Bu).[9] Compound **4** has poor long-range order, as evidenced by the presence of only very broad, weak reflections in the XRPD pattern at *d* spacings of 11.00, 5.40, 4.30, 3.17, and 1.99 Å.

The X-ray structure of the trimethyltin derivative **1** predicts an asymmetric unit with one type of $\mathrm{Me_3Sn}$ environment, in accordance with which in the ^{119}Sn CP MAS NMR spectrum of **1** one fairly sharp singlet at $\delta = 47.9$ ppm is observed. This chemical shift is compatible with the crystallographically determined trigonal-bipyramidal *trans*-$\mathrm{Me_3SnO_2}$ configuration.[10] In agreement with the ^{13}C CP MAS NMR spectrum reported by Behrens et al.,[8] that of **1** shows only one symmetric signal at room temperature ($\delta = 3.80$ ppm), despite there being two nonequivalent methyl carbon atoms in the asymmetric unit. Therefore the $\mathrm{Me_3Sn}$ groups must rotate freely about the O-Sn-O axes on the NMR timescale.[8] Compounds **2** – **5** were also characterized by ^{13}C and ^{119}Sn CP MAS NMR spectroscopy. The tricyclohexyltin derivative **3** gives rise to several sharp or broad overlapping ^{13}C signals in the expected range for $\mathrm{Cy_3Sn}$ species.[11] Compound **4** exhibits

Table 1. Thermogravimetric, ^{119}Sn CP MAS NMR, FTIR, and FT Raman data of the compounds $[(\mathrm{R_3Sn})_2\mathrm{MoO_4}] \cdot n\,\mathrm{H_2O}$ (**1** – **5**) and $\mathrm{Na_2MoO_4 \cdot 2H_2O}$.

Compound	$\mathrm{DTG_{max}}$ [°C]	$\delta(^{119}\mathrm{Sn})$	ν(MoO) and δ(MoO) [cm^{-1}] IR	Raman
1 (R = Me)	297	47.9	856	917, 867, 348, 311
2 (R = *n*Bu)[a]	287	17.9, 20.3	810	924, 860, 308
3 (R = Cy)	262[b]	– 96.7	941, 800	940, 925, 856, 318
4 (R = Ph)	293[c]	–[d]	814	935, 864, 309
5 (R = Bz)	197[e]	– 67.0, – 85.9, – 112.6[f]	835	933, 863, 317
$\mathrm{Na_2MoO_4 \cdot 2H_2O}$	–	–	901, 869, 822	896, 834, 842, 807, 327, 285

[a] See ref. [7]. [b] Starts to melt at 215 °C and decomposes to an orange product. [c] Decomposes to a blue-green product. [d] No resolved signals were observed. [e] Starts to melt at 85 °C, foams at 108 °C. [f] Spectrum acquired with 20000 scans (ca. 22 h).

three resonances at $\delta = 141.9$, 136.1, and 128.2 ppm, attributed to the phenyl carbon atoms. Two resonance ranges are in evidence for the tribenzyltin derivative **5**, at $\delta = 26.8 - 30.2$ and 123.4 – 141.6 ppm, attributed to the methylene carbon and phenyl carbon atoms, respectively. As reported previously,[7] the ^{119}Sn CP MAS NMR spectrum of **2** shows two very close singlets, suggesting the presence of two slightly nonequivalent sites in the asymmetric units (Table 1). Compound **3**, however, exhibits only one ^{119}Sn resonance, indicating the presence of a relatively simple asymmetric unit containing only one type of tin atom. The chemical shift value is consistent with the presence of a five-coordinate tin atom.[11, 12] For the triphenyltin derivative **4** no resolved signals were observed, presumably because of its low crystallinity. The tribenzyltin derivative **5** gave a complicated ^{119}Sn CP MAS NMR spectrum composed of three resolved signals at $\delta = -67.0$, -85.9, and -112.6 ppm. These are shifted markedly upfield relative to the characteristic $\delta(^{119}\mathrm{Sn})$ values for four-coordinate tribenzyltin compounds ($+55$ to -25 ppm), and are in the range typical for five-coordinate compounds.[13] The presence of a fourth signal was also indicated, but it was impossible to decide between lines at $\delta = -115$ and -154 ppm because of the overlapping of peaks and the complex spinning sideband pattern.

Table 1 summarizes the observed Mo–O vibrational frequencies for **1**–**5**. The FTIR spectrum of **1** presents a very strong band at 856 cm^{-1}, which is assigned to the asymmetric stretch of the $[MoO_4]^{2-}$ oxoanion. In the Raman spectrum, this mode is observed with medium intensity at 867 cm^{-1}. The Raman spectrum also contains a strong band at 917 cm^{-1} for the symmetric stretch and bands at lower wavenumbers (348 and 311 cm^{-1}) for the bending modes. The ν and δ(Mo–O) vibrational frequencies for **1** are weakly shifted in comparison with those of $Na_2MoO_4 \cdot 2H_2O$ (Table 1).[8] Despite the local D_{2d} symmetry of each $Mo(OSn)_4$ fragment, the observed vibrational spectrum of the MoO_4 unit follows the selection rules for T_d symmetry.[8, 14] On the whole, these observations also apply to **2**–**5**. The main differences are that the IR-active ν_{asym} mode for **2**–**5** is observed at slightly lower frequency (800 – 835 cm^{-1}), and the Raman-active ν_{sym} mode at higher frequency (924 – 940 cm^{-1}). Hardcastle and Wachs found the correlation between the Raman scattering frequencies of Mo–O bonds and their respective bond lengths in molybdenum oxide compounds[15] to be given by Equation (2).

$$\nu = 32895 \exp(-2.073r) \quad (2)$$

The standard deviation associated with the calculation of a stretching frequency from an Mo–O bond length was ± 25 cm^{-1}. In **1**–**5**, the average Mo–O bond length is 1.77 Å by X-ray diffraction for **1** or EXAFS for **2**–**5** (see below), and inserting this value in Equation (2) gives a value of 839 cm^{-1} for the ν_{sym} mode. This is close to the estimate by Hardcastle and Wachs for the stretching frequency of a perfect MoO_4 tetrahedron (858 cm^{-1}).[15] The observed symmetric stretches for $Na_2MoO_4 \cdot 2H_2O$ and **1**–**5** are considerably higher than these calculated values, indicating the presence of distorted MoO_4 tetrahedra.[15, 16] Accordingly, the vibrational spectra of $Na_2MoO_4 \cdot 2H_2O$ indicate a lowering of the symmetry of the $[MoO_4]^{2-}$ oxoanion.[16] It is surprising that the spectra of **1**–**5** do not follow this trend. A possible exception is **3**, which shows a weak band at 940 cm^{-1} in the FTIR spectrum. This may be attributed to the ν_{sym} mode that has become IR-active because of a reduction of symmetry from T_d.

Mo *K*-edge and Sn *K*-edge extended X-ray absorption fine structure (EXAFS) studies were carried out for **1**–**5** to obtain more detailed structural information on the average local environments of molybdenum and tin. The X-ray crystal structure of **1** is known and therefore it serves as a good model compound.[8] The room-temperature Mo *K*-edge EXAFS of **1** was fitted by a model comprising four oxygen atoms at 1.77 Å (Table 2; Figure 1). The refined coordination number (CN) and distance match the X-ray crystallographic values very

Table 2. Mo *K*-edge and Sn *K*-edge EXAFS-derived structural parameters for $[(Me_3Sn)_2MoO_4]$ (**1**).[a]

Edge	T [K]	Fit	Atom	CN[b]	r [Å]	$2\sigma^2$ [Å]^2[c]	E_f [eV][d]	R [%][e]
Mo *K*	298	A1	O	4.0(2)	1.768(2)	0.0032(2)	1.3(5)	28.0
	30	B1	O	4.0(2)	1.761(2)	0.0028(2)	2.5(5)	30.3
			Sn	2.0(4)	3.824(3)	0.0045(4)		
		B2[f]	O	4.0(2)	1.763(2)	0.0028(2)	1.8(5)	27.9
			Sn	4.0	3.829(3)	0.0064(3)		
		B3[f]	O	4.0(2)	1.763(2)	0.0028(2)	1.8(5)	27.6
			Sn	4.0	3.829(3)	0.0064(3)		
			Mo	8.0(50)	7.391(22)	0.0139(37)		
Sn *K*	30	C1[g]	C	3.0(5)	2.131(7)	0.0061(8)	$-9.6(7)$	46.7
			O	2.0(4)	2.252(8)	0.0062(11)		
			Mo	2.0	3.831(3)	0.0056(4)		
			Sn	4.0(40)	5.601(17)	0.0165(30)		
			Sn	8.0(30)	7.469(6)	0.0079(7)		

[a] Coordination shells and mean interatomic distances [Å] for $[(Me_3Sn)_2MoO_4]$, calculated from the crystal structure(ref. [8]) using the program SEXIE (see ref. [17]) (central atom in italics, coordination number in parentheses): *Mo*···O = 1.770 (4), *Mo*···Sn = 3.839 (4) (Mo-O-Sn = 143.6°), *Mo*···Mo 7.390 (4), *Mo*···Mo 7.466 (4); *Sn*···C = 2.095 (2), *Sn*···C = 2.148 (1), *Sn*···O = 2.269 (2), *Sn*···Mo = 3.839 (2), *Sn*···Sn = 5.626 (4), *Sn*···Sn = 7.390 (4), *Sn*···Sn = 7.463 (4). Maximum deviation for considering atoms to be in a common shell = 0.01 Å. [b] CN = coordination number. Values in parentheses are statistical errors generated in EXCURVE. The true errors in coordination numbers are likely to be of the order of 20%, and those for the interatomic distances ca. 1.5% (see Ref. [18]). [c] Debye – Waller factor; σ = root-mean-square internuclear separation. [d] E_f = edge position (Fermi energy), relative to calculated vacuum zero. [e] $R = (\int[\Sigma^{theory} - \Sigma^{exptl}]k^3 dk / [\Sigma^{exptl}]k^3 dk) \times 100\%$. [f] Multiple scattering calculation for Mo-O-Sn: Mo-O-Sn = 143.7(13)°; maximum pathlength = 10 Å; maximum order of scattering = 3; paths considered = Mo-O-Sn-Mo, Mo-O-Sn-O-Mo. [g] Multiple scattering calculation for Sn-O-Mo: Sn-

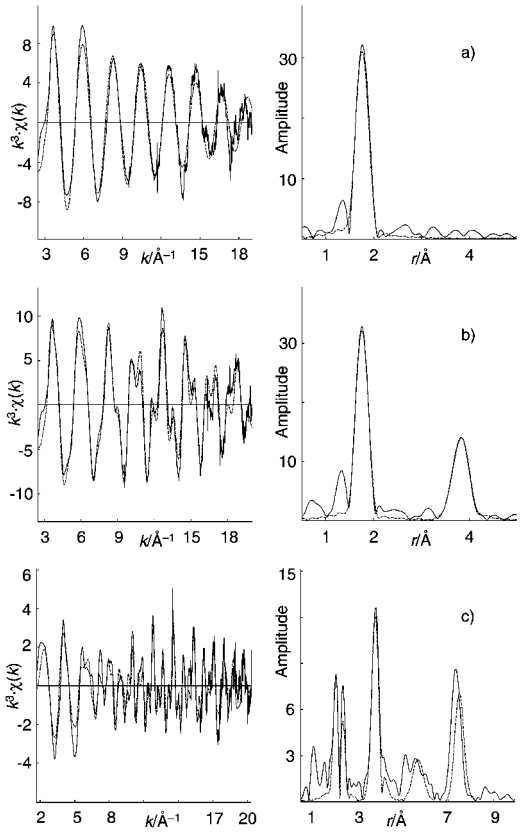

Figure 1. k^3-weighted EXAFS and Fourier transforms of $[(Me_3Sn)_2MoO_4]$ (**1**): a) Mo *K*-edge at 298 K; b) Mo *K*-edge at 30 K; c) Sn *K*-edge at 30 K. The solid lines represent the experimental data and the broken lines show fits using parameters given in Table 2 (fits A1, B2, and C1).

well (see the footnote in Table 2). According to the crystal structure, there is only one type of molybdenum atom in the asymmetric unit. The second coordination shell for this atom consists of four tin atoms at the mean distance of 3.84 Å. However, the Fourier transform (FT) of the room-temperature Mo *K*-edge EXAFS of **1** does not indicate a well-defined second shell close to 4 Å (Figure 1). Cooling the sample down to 30 K had a dramatic effect, leading to the appearance of a new intense peak in the FT just below 4 Å (Figure 1). Fitting this shell as tin with single scattering calculations gave a reasonable result (Mo···Sn = 3.824(3) Å, fit B1 in Table 2), but the refined coordination number of 2.0(4) is much lower than the expected value of 4.0. A much better result was obtained upon inclusion of multiple scattering for the Mo-O-Sn unit (fit B2 in Table 2; Figure 1). The goodness-of-fit *R* factor decreased to 27.9 % and the refined structural parameters, including the Mo-O-Sn angle (143.7(13)°), are in excellent agreement with the X-ray diffraction results. A slight improvement in the overall fit was obtained by addition of eight Mo atoms at 7.4 Å (fit B3; the crystal structure predicts four Mo at 7.39 Å and four Mo at 7.47 Å). Not surprisingly, there are large statistical errors in the refined structural parameters for this distant third shell.

The low-temperature Sn *K*-edge EXAFS of **1** turned out to be very complex and it was difficult to obtain a good fit, even with the five-shell model described in Table 2 (Figure 1). Nevertheless there is excellent agreement (to 1 % or less) between the EXAFS-derived interatomic distances and the single-crystal X-ray values. Once again, multiple scattering was included for the Sn-O-Mo unit (Sn-O-Mo = 144.1(9)°). Overall the results are consistent with the presence of *trans*-R_3SnO_2 units with trigonal-bipyramidal geometry. A crucial finding is that analysis of both the Mo *K*-edge and Sn *K*-edge data gives the same value for the closest Mo···Sn interaction (3.83 Å).

The Mo *K*-edge and Sn *K*-edge EXAFS analysis results for **3** – **5** are detailed in Tables 3 – 5, and Figure 2 illustrates results for compound **4** (other spectra are given in the Supporting information; see also ref. [7] for results concerning **2**). A few general comments apply to the Mo *K*-edge EXAFS-derived structural parameters for all compounds **2** – **5**. The first shell always fits very well as four oxygen atoms at 1.763 – 1.768 Å. This shell is very well defined, characterized by low Debye – Waller factors in the range 0.002 – 0.006 Å^2. Molybdenum is present in all five coordination polymers as tetrahedral

Table 3. Mo *K*-edge and Sn *K*-edge EXAFS-derived structural parameters for $[(Cy_3Sn)_2MoO_4]$ (**3**).

Edge	*T* [K]	Fit	Atom	CN	*r* [Å]	$2\sigma^2$ [Å]^2	E_f [eV]	*R* [%]
Mo *K*	298	A1	O	4.0(1)	1.768(2)	0.0057(2)	0.0(4)	26.3
		A2	O	4.0(1)	1.768(2)	0.0056(2)	0.0(4)	24.4
			Sn	0.7(4)	3.677(10)	0.0095(16)		
		A3	O	4.0(1)	1.768(2)	0.0057(2)	0.1(4)	25.2
			Sn	0.5(4)	3.925(12)	0.0076(18)		
	30	B1	O	4.0(1)	1.768(2)	0.0044(2)	0.3(4)	25.7
		B2	O	4.0(1)	1.768(2)	0.0044(2)	0.2(4)	23.3
			Sn	1.0(4)	3.698(8)	0.0100(13)		
		B3	O	4.0(1)	1.768(2)	0.0044(2)	0.3(4)	23.8
			Sn	0.6(3)	3.999(9)	0.0063(13)		
Sn *K*	298	C1[a]	C	4.7(2)	2.156(2)	0.0090(4)	– 8.6(3)	24.8
			C	4.6(7)	3.083(8)	0.0133(16)		
			C	2.5(7)	3.544(10)	0.0067(18)		
		C2	C	4.7(2)	2.156(2)	0.0090(4)	– 8.6(3)	25.5
			C	4.4(7)	3.083(8)	0.0125(16)		
			Mo	0.5(3)	3.670(10)	0.0108(17)		
		C3	C	4.7(2)	2.156(2)	0.0090(4)	– 8.6(3)	26.8
			C	4.4(7)	3.083(8)	0.0126(17)		
			Mo	0.5(4)	3.991(32)	0.0179(61)		
	30	D1[a]	C	4.6(2)	2.156(2)	0.0071(4)	– 8.2(4)	28.0
			C	5.5(6)	3.081(5)	0.0084(9)		
			C	4.0(10)	3.544(12)	0.0108(24)		
		D2	C	4.6(2)	2.156(2)	0.0072(4)	– 8.3(4)	28.6
			C	5.4(6)	3.081(5)	0.0081(9)		
			Mo	0.8(5)	3.695(12)	0.0141(21)		
		D3	C	4.6(2)	2.156(2)	0.0071(4)	– 8.1(4)	28.5
			C	5.4(6)	3.080(5)	0.0082(9)		
			Mo	0.8(4)	3.992(10)	0.0109(16)		

[a] Two-shell fits (carbon atoms at 2.16 and 3.08 Å) to the room-temperature and low-temperature Sn *K*-edge EXAFS data gave *R* factors of 27.3 % and 30.9 %, respectively.

Table 4. Mo *K*-edge and Sn *K*-edge EXAFS-derived structural parameters for $[(Ph_3Sn)_2MoO_4]\cdot 2H_2O$ (**4**).

Edge	T [K]	Fit	Atom	CN	r [Å]	$2\sigma^2$ [Å]^2	E_f [eV]	R [%]
Mo *K*	298	A1	O	4.0(1)	1.767(2)	0.0041(2)	0.4(4)	26.2
		A2	O	4.0(1)	1.767(2)	0.0041(2)	0.3(4)	25.3
			Sn	1.0(6)	3.752(14)	0.0127(23)		
		A3	O	4.0(1)	1.766(2)	0.0041(2)	0.6(4)	25.1
			Sn	1.0(6)	4.041(13)	0.0110(21)		
Sn *K*	298	B1[a]	C	3.0	2.123(3)	0.0048(5)	−7.6(6)	37.1
			C	6.0(8)	3.071(8)	0.0104(15)		
			C	6.0	4.414(14)	0.0030(27)		
			C	3.0	4.912(20)	0.0076(40)		
		B2[a]	C	3.0	2.123(3)	0.0048(5)	−7.5(6)	35.2
			C	6.0(8)	3.070(8)	0.0104(14)		
			C	6.0	4.410(14)	0.0028(27)		
			C	3.0	4.910(19)	0.0073(38)		
			Mo	1.0(6)	3.731(18)	0.0168(33)		
		B3[a]	C	3.0	2.123(3)	0.0048(5)	−7.7(6)	34.9
			C	6.0(8)	3.072(8)	0.0104(14)		
			C	6.0	4.408(22)	0.0073(48)		
			C	3.0	4.906(21)	0.0083(41)		
			Mo	1.0(7)	4.027(15)	0.0132(27)		
		B4[b]	C	3.0	2.125(3)	0.0050(5)	−8.4(6)	38.2
			C	6.0	3.067(8)	0.0122(14)		
			C	6.0	4.412(16)	0.0116(39)		
			C	3.0	4.923(26)	0.0104(56)		

[a] Multiple scattering calculation for Sn−C1 ··· C4: Sn−C ··· C = 180°; maximum pathlength = 10 Å; maximum order of scattering = 3; paths considered = Sn-C1-C4-Sn, Sn-C1-C4-C1-Sn. Multiple scattering calculation for Sn ··· C2−C3: Sn ··· C−C = 158(7)°; maximum pathlength = 10 Å; maximum order of scattering = 3; paths considered = Sn-C2-C3-Sn, Sn-C2-C3-C2-Sn. [b] A full multiple scattering calculation was performed, using a cluster with D_{3h} point group symmetry generated from the four-shell model. Spherical polar coordinates for shells 1–4 were $\theta_1 = 90°$, $\theta_2 = 66.4°$, $\theta_3 = 73.2°$, $\theta_4 = 90°$, and $\phi_{(1-4)} = 0°$ [θ_i is the angle between the principal axis (z axis) and the line from the central atom to the atom(s) in shell i, and ϕ_i is the angle between an atom in shell i and the x axis]. Maximum pathlength = 10 Å; maximum order of scattering = 3; paths considered = Sn-C1-Sn-C1-Sn, Sn-C1-C1″-Sn, Sn-C1-C2-Sn, Sn-C1-C2-C1-Sn, Sn-C2-C1-C2-Sn, Sn-C1-C2″-Sn, Sn-C1-C3-Sn, Sn-C1-C3-C1-Sn, Sn-C1-C4-Sn, Sn-C1-C4-C1-Sn, Sn-C2-C2′-Sn, Sn-C2-C3-Sn, Sn-C2-C3-C2-Sn (C″ indicates C atom in different phenyl ring; C′ indicates equivalent C atom in the same phenyl ring).

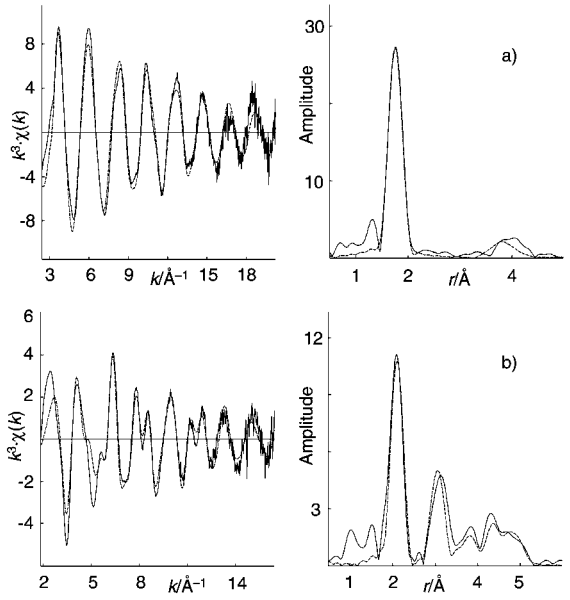

Figure 2. a) Mo *K*-edge and b) Sn *K*-edge k^3-weighted EXAFS and Fourier transforms of $[(Ph_3Sn)_2MoO_4]\cdot 2H_2O$ (**4**). The solid lines represent the experimental data, measured at room temperature, and the broken lines show fits using parameters given in Table 4 (fits A2 and B2).

Table 5. Mo *K*-edge and Sn *K*-edge EXAFS-derived structural parameters for $[(Bz_3Sn)_2MoO_4]\cdot 4H_2O$ (**5**).

Edge	T [K]	Fit	Atom	CN	r [Å]	$2\sigma^2$ [Å]^2	E_f [eV]	R [%]
Mo *K*	298	A1	O	4.0(1)	1.765(2)	0.0043(2)	0.1(4)	23.7
		A2	O	4.0(1)	1.765(2)	0.0043(2)	0.1(4)	22.9
			Sn	0.5(4)	3.735(12)	0.0082(19)		
		A3	O	4.0(1)	1.764(1)	0.0043(2)	0.2(4)	22.8
			Sn	1.0(6)	3.996(13)	0.0120(22)		
	30	B1	O	4.0(1)	1.764(1)	0.0035(2)	0.3(4)	23.7
		B2	O	4.0(1)	1.764(1)	0.0035(2)	0.2(4)	23.1
			Sn	0.5(4)	3.653(24)	0.0124(41)		
		B3	O	4.0(1)	1.764(1)	0.0035(2)	0.3(4)	21.3
			Sn	1.4(6)	3.938(8)	0.0111(13)		
Sn *K*	298	C1[a]	C	5.0(2)	2.152(2)	0.0090(4)	−7.0(3)	24.0
			C	3.0(15)	2.999(30)	0.0382(107)		
			C	2.5(10)	3.512(13)	0.0084(29)		
			Mo	0.4(3)	3.726(14)	0.0104(25)		
		C2	C	5.0(2)	2.152(2)	0.0090(4)	−7.0(3)	23.9
			C	3.0(15)	2.998(29)	0.0379(104)		
			C	2.5(10)	3.539(13)	0.0090(26)		
			Mo	0.4(3)	3.992(12)	0.0089(19)		
	30	D1[b]	C	5.0(2)	2.158(2)	0.0082(4)	−6.4(4)	25.5
			C	3.0(10)	3.035(19)	0.0213(52)		
			C	3.0(9)	3.524(10)	0.0069(18)		
			Mo	0.5(2)	3.941(7)	0.0064(11)		

[a] The R factor decreased from 29.4% to 27.2% upon addition of the second C shell at 3.00 Å, and from 27.2% to 24.9% upon addition of the third C shell at 3.51 Å. [b] The R factor decreased from 35.2% to 32.8% upon addition of the second C shell at 3.04 Å, and from 32.8% to 29.8% upon addition of the third C shell at 3.52 Å.

$[MoO_4]^{2-}$ units. As described above, each Mo atom in **1** has four tin neighbors at 3.83 Å. Compounds **2**–**5** are different in that it is generally possible to fit shells for tin at two different distances, slightly shorter (3.65–3.79 Å) and slightly longer (3.93–4.07 Å) than the corresponding Mo ··· Sn interaction in **1**. The addition of these shells brings about relatively small improvements in the overall fits, and there are large statistical errors in the refined structural parameters, in particular the coordination numbers, which are lower than expected and do not seem to be consistent with the presence of four tin neighbors. However, considerable caution must be attached to the accuracy of these results, partly because of the large statistical errors, and also because the refinement of coordination numbers and Debye–Waller factors simultaneously does not always give reliable results, owing to the high correlation of the two parameters. Measuring the Mo *K*-edge EXAFS spectra of **3** and **5** at low temperature (30 K) did not result in a marked improvement in the definition of the Mo ··· Sn interaction, unlike that seen for **1**, although there were slight reductions in the statistical errors with a concomitant increase in the refined coordination numbers (Tables 3 and 5).

As described previously, the room-temperature Sn *K*-edge EXAFS of **2** could be fitted by a two-shell model composed of 3.5 carbon atoms at 2.14 Å and 2.0 oxygen atoms at 2.26 Å.[7] These distances are very similar to those for **1** and, therefore, support the presence of trigonal-bipyramidal R_3SnO_2 units (with shared oxygen atoms). By contrast, for **3**–**5** it was not possible to fit two separate shells for the first coordination sphere (Tables 3–5). Instead, only one carbon shell was fitted at 2.12–2.16 Å with optimum coordination numbers in the range 4.3–5.0. The coordination number values nevertheless

suggest the presence of five-coordinate tin environments, in agreement with the ^{119}Sn NMR results. That separate shells for carbon and oxygen cannot be fitted is probably due to the similarity of the two elements as backscatterers, and the close proximity of the two shells. The presence of multiple tin environments (especially for **4** and **5**) also complicates the analysis. As found for the Mo *K*-edge data, the FTs of the Sn *K*-edge EXAFS of **2** – **5** indicate the presence of shells around 4 Å. Indeed, it is possible to fit shells for molybdenum at two different distances, slightly shorter (3.67 – 3.76 Å) and slightly longer (3.94 – 4.07 Å) than the corresponding Sn ··· Mo interaction in **1** (3.83 Å). The addition of each shell generally produced statistically significant improvements in the overall fits and the refined Sn ··· Mo distances correlate remarkably well (to within ±0.01 Å in most cases) with the values obtained from the Mo *K*-edge EXAFS data. This confirms quite strongly the coexistence of short (3.65 – 3.79 Å) and long (3.93 – 4.07 Å) Mo ··· Sn interactions in the organotin – oxomolybdate coordination polymers **2** – **5** (Figure 3). A referee

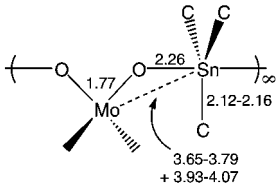

Figure 3. Summary of the EXAFS-derived structural information for the organotin – oxomolybdates **2** – **5**. The Sn–O distance could be determined only for the tri-*n*-butyltin derivative **2**.

suggested that, for the hydrated compounds **4** and **5**, insertion of water into Sn–O bonds to give nonlinear fragments of the type SnO(H)H ··· OMo may be possible. However, there is no convincing evidence for this from the EXAFS data. In particular, the Mo and Sn *K*-edge EXAFS results concerning the nonbonded Sn ··· Mo interactions for the anhydrous compounds **2** – **3** are not very different from those of the hydrated compounds **4** – **5**.

For the Sn *K*-edge EXAFS of **3**, a shell for carbon atoms at 3.08 Å could be fitted in addition to the shells described above (Table 3). The best coordination number for this shell was about 4.5 for the room-temperature data, rising to 5.5 for the low-temperature data. This is consistent with the presence of tricyclohexyltin environments. The Sn ··· C distance seems reasonable when compared with that reported for *trans*-dichlorotricyclohexylarsenic(v), $[AsCl_2(C_6H_{11})_3]$ (As ··· C = 2.84 – 2.99 Å; As–C = 1.99 Å).[19] The FTs of the Sn *K*-edge EXAFS of **3** recorded at different temperatures indicate the presence of an additional shell at about 3.5 Å. This was best fitted as either 2.5 (298 K, fit C1) or 4 (30 K, fit D1) carbon atoms at 3.54 Å. However, this distance does not seem plausible, considering that the X-ray crystal structure of the $[AsCl_2(C_6H_{11})_3]$ mentioned above reveals the next significant shell of carbon atoms after those at 2.84 – 2.99 Å to be at 4.26 – 4.33 Å. At present, we are unable to offer an attribution for this shell. Curiously, the same shell is also in evidence for the tribenzyltin derivative **5**, in addition to a shell of three carbon atoms at 3.0 Å (Table 5). The distance for the latter shell is similar to that reported for tribenzyltin chloride.[20] According to the X-ray crystal structure of this compound, the next shell of carbon atoms after that at 3.03 Å is at 3.69 Å (CN = 3). Therefore, once again, the 3.5 Å shell for **5** seems rather short to be assigned to CH carbon atoms of the phenyl groups.

The room-temperature Sn *K*-edge EXAFS and FT for compound **4** are shown in Figure 2. The data were initially modeled with four carbon shells at 2.12, 3.07, 4.41, and 4.91 Å (fit B1, Table 4). Although the best value for the coordination number of the first shell was 4.3(2), this was fixed at 3.0 so that multiple scattering could be included in the calculations for the linear Sn–C ··· C unit (2.12 and 4.91 Å, Sn–C ··· C = 180°). A separate unit was also defined for the other two carbon atoms (3.07 and 4.41 Å, Sn ··· C–C = 158°). The refined Sn ··· C distances are in the expected range for triphenyltin species.[21] Satisfactory fitting of the two shells at 4.41 and 4.91 Å could not be achieved without multiple scattering included. The EXAFS fits were further improved by addition of shells for molybdenum at either 3.73 (fit B2) or 4.03 Å (fit B3). Returning to the four-shell model, as an alternative to defining two separate units for the multiple scattering calculations, a full multiple scattering calculation by using the so-called cluster method was achieved by starting with the four-shell model described above and in Table 4. For each shell, the position of one particular atom was defined by spherical polar coordinates θ and ϕ, values for which were determined from the above unit-method theoretical fits (Table 4). A D_{3h} symmetry operation was then performed to generate the complete cluster. The structural parameters (Debye – Waller factors, interatomic distances, and E_f) were then refined with multiple scattering calculated for paths between all atoms, including those through the central atom (up to a maximum pathlength of 10 Å). The final cluster is represented in Figure 4. The interatomic distances are reasonable, including the calculated C–C bond lengths for the aromatic rings (1.4 Å). However, the overall fit, as judged by the *R* factor, is not better than that achieved using the simple (and computationally much faster) unit method.

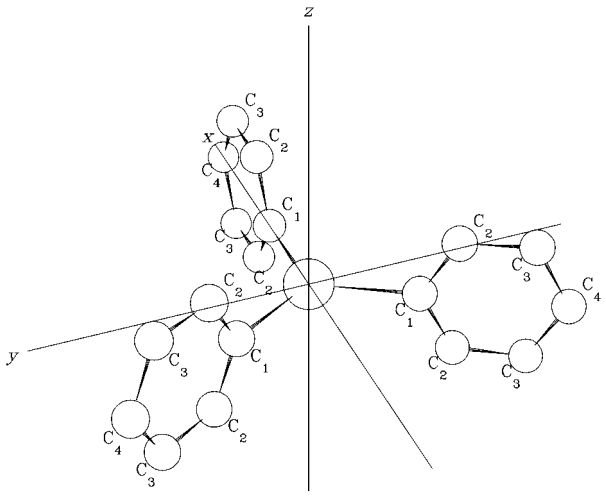

Figure 4. Representation of the final cluster with D_{3h} symmetry used to model the room-temperature Sn *K*-edge EXAFS of **4** with full multiple scattering included in the calculations (fit B4, Table 4).

Sulfoxidation catalysis in the presence of 1–5: The oxidation of benzothiophene was carried out with aqueous hydrogen peroxide in the presence of compounds **1**–**5** at 35 °C and atmospheric pressure, with water, acetonitrile, ethanol, or 1,2-dichloroethane as additional co-solvent (substrate/oxidant/catalyst = 100:200:1). Control experiments showed that benzothiophene oxidation did not take place to a measurable extent in the absence of **1**–**5**. In the most favorable case (**2** as catalyst precursor and 1,2-dichloroethane as co-solvent), conversion of benzothiophene reached 57% within one hour (Figure 5). The nature of the additional solvent has an

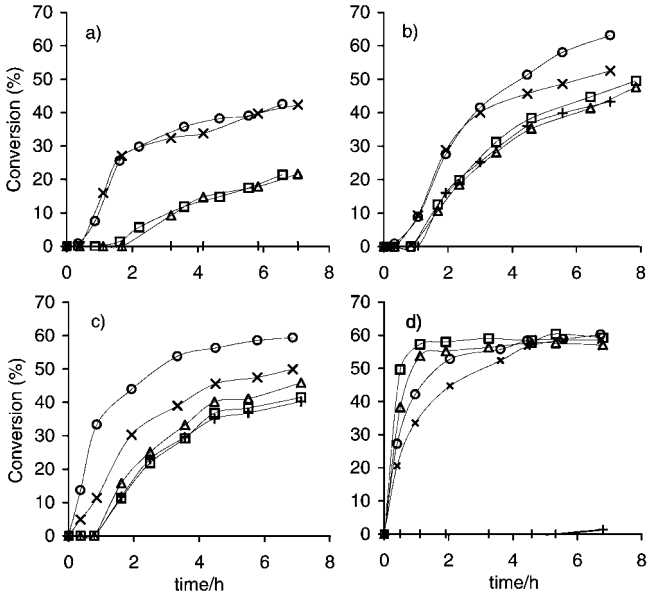

Figure 5. Kinetics of benzothiophene oxidation with aqueous H_2O_2 at 35 °C in the presence of the organotin–oxomolybdates **1** (+), **2** (□), **3** (△), **4** (×) and **5** (○), using a) water, b) acetonitrile, c) ethanol, or d) 1,2-dichloroethane as co-solvent. Molar ratio substrate/oxidant/catalyst = 100:200:1.

important effect on yields and reaction kinetics, although this effect is strongly dependent on the catalyst type (Figure 5). Regardless of the type of catalyst precursor or additional solvent, the reactions were highly selective and led directly to the sulfone (1,1-dioxide), even for low levels of substrate conversion [Eq. (3)]. Only traces of sulfoxides were found among the oxidation products.

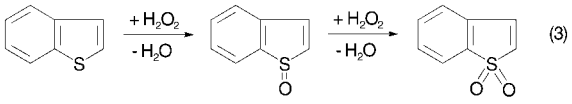

(3)

Some properties of the different catalyst systems need to be borne in mind when interpreting the oxidation results. With water as the only solvent, two liquid phases are present as benzothiophene is insoluble in water. For this system it was noted that the catalyst precursors **4** and **5** dissolve readily, whereas **1**–**3** are insoluble (forming solid–liquid–liquid (S–L–L) systems). Acetonitrile and ethanol are fully miscible with the substrate and the hydrogen peroxide solution, forming a single liquid phase. With acetonitrile, the polymers **1**–**3** appear to dissolve slightly during the reaction, and compounds **4** and **5** are even more soluble. In the ethanol-containing system, the trimethyltin derivative is soluble, whereas the other compounds exhibit poor or only partial solubility. 1,2-Dichloroethane dissolves the substrate, but is immiscible with the hydrogen peroxide solution, leading to the formation of two liquid phases. For this system, **1** is very soluble, **2** and **3** only partially so, and **4** and **5** are insoluble.

The turnover frequencies of benzothiophene conversion at 35 °C (calculated for the first 2 h of reaction) vary according to the type of co-solvent and generally increase in the order water < acetonitrile < ethanol < 1,2-dichloroethane (Figure 6). This trend parallels the decrease in solvent polarity, as indicated by the dielectric constants (ε) at 25 °C: water

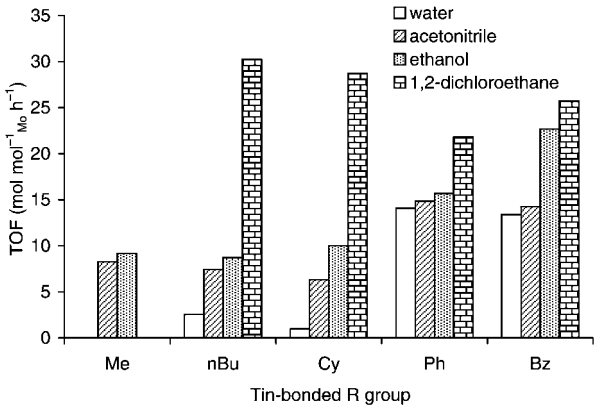

Figure 6. Turnover frequencies of benzothiophene conversion at 35 °C (calculated for the first 2 h of reaction) for the different catalyst precursors, in different co-solvents.

(80.10) > acetonitrile (35.94) > ethanol (24.55) > 1,2-dichloroethane (10.42). In water, long induction periods (up to 100 min) are observed, which become shorter for acetonitrile and ethanol and are not observed for 1,2-dichloroethane (except for **1**). This phenomenon may be related to the different coordinating powers of the solvent molecules. Thus, H_2O and MeCN may compete with peroxide molecules for coordination to the Lewis acidic Mo^{VI} center. This will clearly have a detrimental effect if, as is the case for H_2O_2-based epoxidations of olefins with Mo^{VI} complexes, coordination of the oxidant to the metal center is necessary to generate an electrophilic oxygen atom.[22, 23] Nucleophilic attack of the electron-rich sulfur atom of the substrate on the peroxidic oxygen atom of the intermediate species may then take place, yielding the sulfoxide, which may subsequently be oxidized to the corresponding sulfone.[23–25] Relative to H_2O and MeCN, alcohols are relatively weak ligands and, therefore, may compete less with the oxidant for coordination to molybdenum, resulting in a higher initial activity. The use of a noncoordinating solvent, namely 1,2-dichloroethane, facilitates achievement of the highest initial oxidation rates.

When 1,2-dichloroethane is used as the co-solvent, the initial sulfoxidation rates increase in the order **4** < **5** < **3** < **2**. However, as noted above, the polymers **2** and **3** partially dissolve in this system and the catalysis could be homogeneous. In terms of ease of catalyst separation from the

reaction products, the system that includes the tribenzyltin derivative **5**, which gives practically the same benzothiophene conversion after 6.5 h (approximately 60%), is a more attractive alternative, since for this system the solid catalyst could be separated easily from the liquid phase by centrifuging. After being washed thoroughly with 1,2-dichloroethane, the solid was reused in a second reaction cycle. Benzothiophene conversion after 7 h was 57%, compared with 60% obtained with the fresh catalyst, indicating no significant loss of activity. When the reaction is carried out without substrate, with **5** and 1,2-dichloroethane as co-solvent at 35 °C, the nonproductive decomposition of H_2O_2 measured after 4 h is approximately 10%. In all the above experiments the total amount of peroxide was added at the beginning and the H_2O_2/benzothiophene molar ratio was 2:1. A three-fold increase in this ratio does not change product selectivity, but raises conversion in increments which increase with the reaction time (Figure 7). A further increase in this ratio to 10:1 leads to

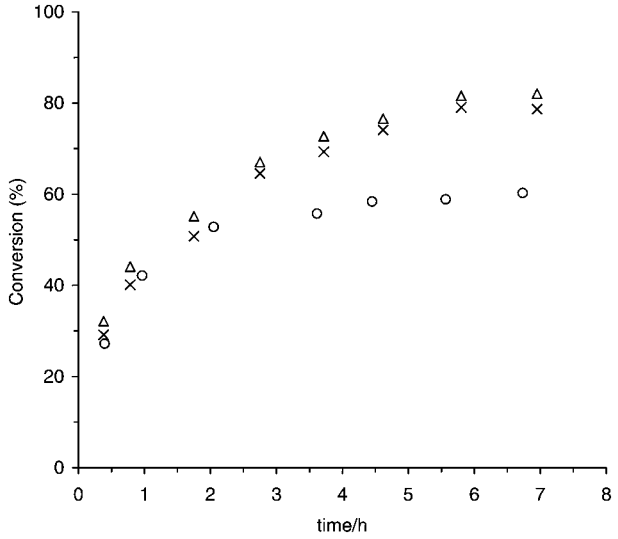

Figure 7. Effect of oxidant concentration on benzothiophene oxidation at 35 °C in the presence of $[(Bz_3Sn)_2MoO_4]\cdot 4H_2O$ (**5**), with 1,2-dichloroethane as co-solvent: Initial H_2O_2/substrate molar ratio = 2:1 (○), 6:1 (△) and 10:1 (×).

a slight decrease in benzothiophene conversion. After reaction for 24 h the sulfone is obtained in quantitative yield. Apparent activation energies of sulfoxidation for the catalyst systems involving **5** were determined in the temperature range 35 – 65 °C (Figure 8). Higher reaction temperatures improved benzothiophene conversion without affecting selectivity. In accordance with the above observations on use of different solvents, the activation energy of sulfoxidation increased from 5 kcal mol^{-1} with 1,2-dichloroethane to 27 kcal mol^{-1} with water.

The catalyst systems containing the derivatives **1** – **3** generally exhibit similar kinetic profiles for a given co-solvent (Figure 5). However, anomalous behavior is exhibited by **1** in the presence of water as only solvent (S – L – L system), for which no conversion of benzothiophene was observed. As described above, the polymers **1** – **3** crystallize as anhydrous compounds. Given that **1** has a layered structure, a possible

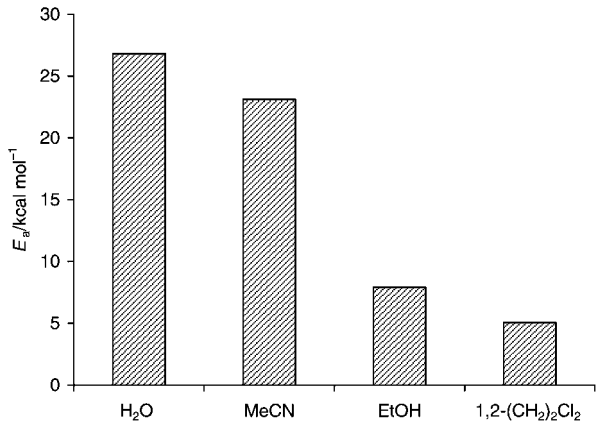

Figure 8. Apparent activation energy of benzothiophene oxidation in the presence of $[(Bz_3Sn)_2MoO_4]\cdot 4H_2O$ (**5**), using different co-solvents.

explanation for the poor performance is that diffusion of substrate and/or oxidant molecules between the layers is hindered by the hydrophobic character of the interlamellar space. The systems containing **2** and **3** may exhibit an induction period for the same reason, but in these cases the bulkier *n*-butyl and cyclohexyl groups probably give rise to a more open structure, thereby facilitating eventual intercalation of reactant molecules. This might be a better explanation for the induction periods observed in the presence of water, acetonitrile, or ethanol (instead of with the competing influence of coordinating solvent molecules). Thus, the polymers **4** and **5** crystallize as hydrated compounds and mass transfer of reactants in the presence of polar solvents may not be so limiting, resulting in higher initial sulfoxidation activities. The kinetic curves demonstrate that, for a given co-solvent, differences in activity are concentrated in the first 1 – 2 h of reaction, after which the observed reaction rates are comparable for all the compounds **2** – **5**. The trimethyltin derivative **1** in the presence of 1,2-dichloroethane exhibits a very long induction period of 6 h, after which benzothiophene conversion increases to 46% after reaction for 24 h. As mentioned above, **1** immediately starts to dissolve in this reaction mixture. The long induction period may be associated with the formation of catalytically active species in solution.

Concluding Remarks

In this work, the $[(R_3Sn)_2MoO_4]$ family of compounds has been extended to include novel tricyclohexyltin and tribenzyltin derivatives. The physicochemical characterization of these compounds, and also of those with R = *n*-butyl and phenyl, points to the formation of coordination polymers in the solid state, in which tetrahedral $[MoO_4]^{2-}$ subunits are linked through $[R_3Sn]^+$ spacers. These compounds are interesting candidates as catalysts or catalyst precursors for oxidation reactions. We have shown that benzothiophene can be oxidized selectively to the corresponding sulfone with aqueous hydrogen peroxide. The catalysis results depend on the complex interplay between various factors, such as the addition of co-solvents and the hydrophobic/hydrophilic

properties of the starting polymers. Changing the nature and size of the tin-bound R groups influences catalytic performance, by inducing structural changes and modifying the surface polarity/polarizability of the compounds. Future work will center on the application of the sulfoxidation reaction with hydrogen peroxide to remove sulfur from petroleum products.

Experimental Section

Microanalyses were performed at the ITQB, Oeiras (C. Almeida). Thermogravimetric analysis studies were performed using a Mettler TA3000 system at a heating rate of 5 °C min^{-1} under nitrogen. Powder XRD data were collected on a Philips X'pert diffractometer with $Cu_{K\alpha}$ radiation filtered by Ni. Infrared spectra were recorded in the range 400–4000 cm^{-1} on a Unican Mattson Mod 7000 FTIR spectrometer with KBr pellets. Raman spectra were recorded on a Bruker RFS 100/S FT Raman spectrometer using 1064 nm excitation of the Nd/YAG laser. Room-temperature ^{13}C and ^{119}Sn NMR spectra were recorded in the solid state at 100.62 and 149.21 MHz, respectively, on a Bruker Avance 400(9.4 T) spectrometer. ^{13}C CP MAS NMR spectra were recorded with a 4.5 μs ^{1}H 90° pulse, 2 ms contact time, a spinning rate of 8 kHz, and 4 s recycle delays. ^{119}Sn CP MAS NMR spectra were recorded with a 3.5 μs ^{1}H 90° pulse, 3 ms contact time, a spinning rate of 6–10 kHz and 4 s recycle delays. For **5**, one ^{119}Sn MAS NMR spectrum was also recorded, using a spinning rate of 15 kHz and 40 s recycle delays (4050 scans). Chemical shift references were $SiMe_4$ and $SnMe_4$. ^{13}C and ^{119}Sn NMR spectra were also recorded in the solid state at 125.76 and 186.50 MHz, respectively, on a Bruker Avance 500 spectrometer.

Mo *K*-edge and Sn *K*-edge X-ray absorption spectra were measured at room temperature or approximately 30 K (in an Oxford Instruments cryostat filled with He exchange gas) in transmission mode on beamline BM29 at the ESRF (Grenoble),[26] operating at 6 GeV in ⅔ filling mode with typical currents of 170–200 mA. The one scan that was performed for each sample was set up to record the pre-edge in 5 eV steps and the post-edge region in 0.025–0.05 Å^{-1} steps, giving a total acquisition time of approximately 45 min per scan. The order-sorting double Si(3 1 1) crystal monochromator was detuned by 40 % to ensure harmonic rejection. Solid samples were diluted with BN and pressed into 13 mm pellets. Ionization chamber detectors were filled with Kr to give 30 % absorbing I_o (incidence) and 70 % absorbing I_t (transmission). The programs EXCALIB and EXBACK (SRS Daresbury Laboratory, UK) were used in the usual manner for calibration and background subtraction of the raw data. EXAFS curve-fitting analyses, by least-squares refinement of the non-Fourier filtered k^3-weighted EXAFS data, were carried out with the program EXCURVE (EXCURV98 version[27]) by using fast curved wave theory.[28] Phase shifts were obtained within this program by ab-initio calculations based on the Hedin Lundqvist/von Barth scheme. Unless otherwise stated, the calculations were performed with single scattering only.

The precursors $Na_2MoO_4 \cdot 2H_2O$, Me_3SnCl, and Ph_3SnCl were obtained from Aldrich and recrystallized before use. Literature methods were used to prepare Bz_3SnCl[29] and Cy_3SnCl.[30] The tri-*n*-butyltin(IV) derivative $[(nBu_3Sn)_2MoO_4]$ (**2**) was prepared as described previously.[7, 8]

Preparation of $[(Me_3Sn)_2MoO_4]$ (1): A saturated solution of $Na_2MoO_4 \cdot 2H_2O$ (1.21 g, 5 mmol) in water (7.0 mL) was added dropwise with stirring to a solution of Me_3SnCl (1.99 g, 10 mmol) in water (5.0 mL). A colorless precipitate was formed immediately and stirring was continued for 5 min. The precipitate was filtered, washed thoroughly with water, and air-dried at 100 °C overnight. Yield: 86 % (2.09 g); IR (KBr): $\tilde{\nu}$ = 2997 (m), 2920 (s), 1749 (w), 1707 (w), 1400 (m), 1261 (w), 1195 (w), 1190 (s), 856 (vs), 725 (vs), 555 cm^{-1} (vs; ν_{as} Sn–C); Raman: $\tilde{\nu}$ = 3001 (w), 2924 (s), 1214 (m), 1188 (w), 917 (s), 867 (m), 555 (s; ν_{as} Sn–C), 525 (vs; ν_s Sn–C), 348 (w), 311 (w), 142 cm^{-1} (s); ^{13}C CP MAS NMR (8 kHz, 25 °C): δ = 3.8 ppm; elemental analysis calcd (%) for $C_6H_{18}O_4MoSn_2$ (487.53): C 14.78, H 3.72; found: C 14.66, H 3.65.

Preparation of $[(Cy_3Sn)_2MoO_4]$ (3): A saturated solution of $Na_2MoO_4 \cdot 2H_2O$ (0.72 g, 3 mmol) in water (4.5 mL) was added dropwise with stirring to a mixture of Cy_3SnCl (2.40 g, 6 mmol) in acetone (40 mL). A colorless precipitate was formed immediately and stirring was continued for 5 min. The precipitate was filtered, then washed thoroughly with water and cold acetone. The compound dried spontaneously overnight at room temperature and was dried further under vacuum. Yield: 80 % (2.14 g); IR (KBr): $\tilde{\nu}$ = 2918 (vs), 2846 (s), 1444 (s), 1259 (m), 1171 (m), 991 (m), 941 (w), 881 (m), 843 (m), 800 (vs), 661 cm^{-1}(m); Raman: $\tilde{\nu}$ = 2928 (vs), 2847 (vs), 1439 (m), 1339 (w), 1295 (w), 1269 (w), 1258 (w), 1172 (m), 1080 (w), 1042 (w), 1022 (m), 992 (w), 940 (m), 925 (w), 880 (m), 856 (w), 842 (m), 806 (m), 649 (s), 487 (w), 419 (w), 318 (w), 298 (w), 239 (w), 189 (s), 88 cm^{-1} (w); ^{13}C CP MAS NMR (8 kHz, 25 °C): δ = 37.2, 35.9, 34.3, 32.9, 31.8, 29.8, 29.6, 29.4, 28.1, 27.5, 26.3 ppm; elemental analysis calcd (%) for $C_{36}H_{60}O_4MoSn_2$ (890.20): C 48.57, H 6.79; found C 48.68, H 7.13.

Preparation of $[(Ph_3Sn)_2MoO_4] \cdot 2H_2O$ (4): A saturated solution of $Na_2MoO_4 \cdot 2H_2O$ (1.21 g, 5 mmol) in water (7.5 mL) was added dropwise with stirring to a solution of Ph_3SnCl (3.85 g, 10 mmol) in acetone (18 mL). The colorless precipitate that was formed immediately was isolated, washed, and dried as for **3**, above. Yield: 85 % (3.58 g); IR (KBr): $\tilde{\nu}$ = 3066 (m), 3047 (m), 1955 (w), 1882 (w), 1819 (w), 1479 (m), 1429 (s), 1076 (m), 999 (m), 812 (vs), 727 (s), 696 (s), 453 cm^{-1}(s); Raman: $\tilde{\nu}$ = 3139 (vw), 3051 (s), 1580 (m), 1481 (w), 1431 (w), 1332 (w), 1192 (w), 1158 (w), 1023 (m), 1002 (vs), 935 (m), 864 (m), 655 (m), 618 (w), 309 (m), 275 (w), 213 (s), 100 cm^{-1} (s); ^{13}C CP MAS NMR (8 kHz, 25 °C): δ = 141.9, 136.1, 128.2 ppm; elemental analysis calcd (%) for $C_{36}H_{34}O_6MoSn_2$ (895.99): C 48.26, H 3.81; found: C 47.77, H 3.52.

Preparation of $[(Bz_3Sn)_2MoO_4] \cdot 4H_2O$ (5): A saturated solution of $Na_2MoO_4 \cdot 2H_2O$ (0.72 g, 3 mmol) in water (4.5 mL) was added dropwise with stirring to a solution of Bz_3SnCl (2.56 g, 6 mmol) in acetone (36 mL). A colorless precipitate that was formed immediately quickly redissolved. The acetone was evaporated to give a colorless elastic solid suspended in the aqueous phase. After treatment with ultrasound, the white powder obtained was filtered and washed with cold acetone. The compound was left to dry overnight at room temperature and turned pale yellow upon further drying in vacuo (drying at higher temperatures degrades the product). Yield: 72 % (2.19 g); IR (KBr): $\tilde{\nu}$ = 3078 (w), 3057 (m), 3020 (m), 2920 (w), 1637 (m), 1597 (s), 1491 (vs), 1452 (s), 1402 (m), 1207 (m), 1108 (w), 1055 (m), 1030 (m), 872 (m), 835 (vs), 798 (m), 758 (vs), 727 (s), 708 (vs), 696 (vs), 619 (w), 551 (w), 451 cm^{-1} (m); Raman: $\tilde{\nu}$ = 3156 (w), 3057 (s), 2974 (w), 2929 (w), 1599 (s), 1581 (w), 1492 (w), 1452 (w), 1407 (w), 1335 (vw), 1209v (s), 1155 (m), 1121 (s), 1107 (s), 1031 (m), 1001 (vs), 933 (m), 863 (w), 800 (w), 621 (w), 582 (w), 563 (s), 435 (s), 317 (m), 225 (m), 203 (m), 114 cm^{-1} (s); ^{13}C CP MAS NMR (8 kHz, 25 °C): δ = 141.6, 140.1, 139.3, 137.6, 128.6, 125.7, 125.0, 124.2, 123.4 (all phenyl C), 30.2, 28.6, 26.8 ppm (all CH_2); elemental analysis calcd (%) for $C_{42}H_{50}O_8MoSn_2$ (1016.18): C 49.64, H 4.96; found: C 49.13, H 4.40.

Catalytic sulfoxidation in the presence of 1–5: Catalytic oxidation of benzothiophene was performed under air (atmospheric pressure) in a reaction vessel equipped with a magnetic stirrer, immersed in a thermostated oil bath at 35 °C. The catalyst/substrate molar ratio was 1 % (36 μmol coordination polymer/3.6 mmol benzothiophene) and the benzothiophene/hydrogen peroxide (30 % aqueous) molar ratio was 0.5:1, with 4 mL solvent. Samples were withdrawn periodically and analyzed in a gas chromatograph (Varian 3800) equipped with a capillary column (SPB-5, 20 m × 0.25 mm × 0.25 mm) and a flame ionization detector. The substrate was quantified by using a calibration curve and undecane as internal standard (added after the reaction). Hydrogen peroxide was quantified by standard iodometric titration.

Acknowledgement

This work was mainly funded by FCT, POCTI and PRAXIS XXI (including a Ph.D. grant to M.A. and postdoctoral grants to A.A.V. and M.P.). We acknowledge the European Synchrotron Radiation Facility for provision of synchrotron radiation facilities and we thank Stuart Ansell for assistance in using beamline BM29. Cláudia Morais and Paula Esculcas are thanked for assistance with the NMR experiments.

[1] D. D. Whitehurst, T. Isoda, I. Mochida, *Adv. Catal.* **1998**, *42*, 345.
[2] R. Shafti, G. J. Hutchings, *Catal. Today* **2000**, *59*, 423.
[3] A. M. Aitani, M. F. Ali, H. H. Al-Ali, *Petrol. Sci. Technol.* **2000**, *18*, 537.
[4] K. N. Brown, J. H. Espenson, *Inorg. Chem.* **1996**, *35*, 7211.
[5] a) M. Te, C. Fairbridge, Z. Ring, *Appl. Catal. A* **2001**, *219*, 267; b) F. M. Collins, A. R. Lucy, C. Sharp, *J. Mol. Catal. A* **1997**, *117*, 397.
[6] V. Hulea, F. Fajula, J. Bousquet, *J. Catal.* **2001**, *198*, 179.
[7] M. Abrantes, A. A. Valente, M. Pillinger, I. S. Gonçalves, J. Rocha, C. C. Romão, *J. Catal.* **2002**, *209*, 237.
[8] U. Behrens, A. K. Brimah, K. Yünlü, R. D. Fischer, *Angew. Chem.* **1993**, *105*, 117; *Angew. Chem. Int. Ed. Engl.* **1993**, *32*, 82.
[9] E. Siebel, R. D. Fischer, *Chem. Eur. J.* **1997**, *3*, 1987.
[10] P. Schwarz, E. Siebel, R. D. Fischer, N. A. Davies, D. C. Apperley, R. K. Harris, *Chem. Eur. J.* **1998**, *4*, 919.
[11] M. Ashfaq, A. Majeed, A. Rauf, A. W. K. Khanzada, W. U. Shah, M. I. Ansari, *Bull. Chem. Soc. Jpn.* **1999**, *72*, 2073.
[12] S. J. Blunden, R. Hill, *Inorg. Chim. Acta* **1985**, *98*, L7.
[13] A. Lyčka, J. Jirman, A. Koloničný, J. Holeček, *J. Organomet. Chem.* **1987**, *333*, 305.
[14] G. Busca, *J. Raman Spectrosc.* **2002**, *33*, 348.
[15] F. D. Hardcastle, I. E. Wachs, *J. Raman Spectrosc.* **1990**, *21*, 683.
[16] V. P. M. Pillai, T. Pradeep, M. J. Bushiri, R. S. Jayasree, V. U. Nayar, *Spectrochim. Acta Part A* **1997**, *53*, 867.
[17] B. Rupp, B. Smith, J. Wong, *Comput. Phys. Commun.* **1992**, *67*, 543.
[18] J. Evans, J. T. Gauntlett, J. F. W. Mosselmans, *Faraday Discuss. Chem. Soc.* **1990**, *89*, 107.
[19] S. Pascu, L. Silaghi-Dumitrescu, A. J. Blake, W.-S. Li, I. Haiduc, D. B. Sowerby, *Acta Crystallogr. Sect. C* **1998**, *54*, 219.
[20] S. W. Ng, *Acta Crystallogr. Sect. C* **1997**, *53*, 56.
[21] S. W. Ng, *Acta Crystallogr. Sect. C* **1999**, *55*, 523.
[22] V. Hulea, P. Moreau, *J. Mol. Catal.* **1996**, *113*, 499.
[23] O. Bortolini, S. Campestrini, F. Di Furia, G. Modena, *J. Org. Chem.* **1987**, *52*, 5093.
[24] M. Madesclaire, *Tetrahedron* **1986**, *42*, 5459.
[25] P. Moreau, V. Hulea, S. Gomez, D. Brunel, F. Di Renzo, *Appl. Catal.* **1997**, *155*, 253.
[26] A. Filipponi, M. Borowski, D. T. Bowron, S. Ansell, A. D. Cicco, S. D. Panfilis, J.-P. Itiè, *Rev. Sci. Instrum.* **2000**, *71*, 2422.
[27] N. Binsted, EXCURV98, CCLRC Daresbury Laboratory computer programme, **1998**.
[28] a) S. J. Gurman, N. Binsted, I. Ross, *J. Phys. C* **1984**, *17*, 143; b) S. J. Gurman, N. Binsted, I. Ross, *J. Phys. C* **1986**, *19*, 1845.
[29] K. Sisido, V. Takeda, Z. Kinugawa, *J. Am. Chem. Soc.* **1961**, *83*, 538.
[30] *Methoden Org. Chem. (Houben-Weyl) 4th ed. 1978*, Vol. XIII/6.

Received: September 6, 2002 [F4399]

